Operational Noise Characterization and Band-Integrated Detection Limits of a Thermo-Formed Piezoelectret Accelerometer

Igor Nazareno Soares*, Ruy Alberto Corrêa Altafim*, Ruy Alberto Pisani Altafim†
*Department of Electrical and Computer Engineering, Engineering School of São Carlos
University of São Paulo
São Carlos, Brazil
†Department of Computer Systems, Informatics Center
Federal University of Paraíba
João Pessoa, Brazil
e-mail: igor.soares@usp.br, altafim@usp.br, ruy@ci.ufpb.br

***Abstract*—Thermo-Formed Piezoelectret Accelerometers (TFPAs) have recently emerged as mechanically tunable vibration sensors. While previous studies have demonstrated their sensitivity and structural tunability, the stochastic limits of vibration detection have not yet been experimentally quantified. This work presents an operational noise characterization and band-integrated detection limit analysis of a TFPA under controlled sinusoidal excitation. The sensor was excited between 50 Hz and 3200 Hz with an acceleration amplitude of 9.81 m/s^2 (1 g). Deterministic signal components were separated from stochastic fluctuations using harmonic regression, and the residual signals were analyzed through Welch Power Spectral Density (PSD) estimation to obtain the operational noise spectrum. The equivalent acceleration noise density was found to remain on the order of 10^{-4} g/$\sqrt{\text{Hz}}$ across most of the analyzed frequency range. Band-integrated analysis yielded detection limits of approximately 3.09 mg Root-Mean-Square (RMS) in the 50–250 Hz band and 22.42 mg RMS over the full 50–3200 Hz range for a unity Signal-to-Noise Ratio (SNR) criterion. These results establish the stochastic performance limits of the TFPA and provide a quantitative assessment of its operational vibration detection capability under the present measurement conditions, thereby contributing to a more complete evaluation of TFPAs as mechanically tunable sensors for practical vibration monitoring applications.**

Keywords*- *Piezoelectret accelerometer; Vibration sensing; Operational noise characterization; Detection limits; Power spectral density; Harmonic regression.

I. INTRODUCTION

Piezoelectret-based sensing technologies have emerged as a lightweight and cost-effective alternative to conventional piezoelectric accelerometers. Owing to their electret charge storage capability and mechanically compliant polymer structures, piezoelectrets enable geometrically tunable transduction mechanisms that are attractive for vibration sensing applications [1]–[3].

Recently, a Thermo-Formed Piezoelectret Accelerometer (TFPA) architecture based on an open tubular polymer electret structure fabricated by thermo-forming was introduced and experimentally validated, demonstrating adjustable dynamic response through seismic mass variation and structural configuration [4][5]. Subsequent investigations provided extended dynamic characterization under controlled excitation conditions [6] and demonstrated the tunability and application potential of the device in domain-specific scenarios such as agricultural monitoring [7]. Collectively, these studies established the TFPA platform in terms of design, dynamic response, and application-oriented tunability.

While sensitivity and frequency response are fundamental performance metrics [8], they are not sufficient to fully characterize the detection capability of a dynamic sensor. The minimum measurable acceleration level is limited by stochastic noise contributions originating from the sensing structure, the transduction mechanism, the signal conditioning electronics, and the data acquisition chain [9]. In accelerometer research, noise is often reported as voltage noise density or equivalent acceleration noise density, typically measured under quiescent or unloaded conditions. However, practical sensing scenarios commonly involve operation under dynamic excitation, where deterministic vibration components coexist with stochastic fluctuations.

When a sensor is subjected to controlled sinusoidal excitation, the measured output contains a deterministic component phase-locked to the excitation frequency, potentially accompanied by higher-order harmonics arising from nonlinearities. Superimposed on these components is a stochastic contribution that represents operational noise. If deterministic components are not explicitly removed, Power Spectral Density (PSD) estimates may be biased, particularly near the excitation frequency, leading to inaccurate noise quantification [10]. Furthermore, detection limits derived from spectral quantities depend on the frequency band over which noise is integrated, emphasizing the importance of band-specific evaluation rather than single-value noise floor reporting [11].

To address these aspects, the present study adopts a signal processing framework for operational noise characterization under sinusoidal excitation. The deterministic component at the excitation frequency and its harmonics is estimated via harmonic regression using sine–cosine basis functions and subsequently removed from the measured signal. The residual signal is then analyzed using Welch PSD estimation [10] to obtain the voltage noise density. By combining the residual spectral density with the sensitivity estimated through harmonic regression, an equivalent acceleration noise density is derived. Band-integrated Root-Mean-Square (RMS) noise

levels are subsequently obtained by integrating the equivalent acceleration noise density over specified frequency intervals, from which the corresponding detection limits are derived [11]. In addition, the analysis accounts for heterogeneous acquisition sampling rates by interpolating spectra onto a common frequency grid bounded by the minimum Nyquist frequency.

Using this approach, the operational noise characteristics and band-integrated detection limits of a TFPA equipped with a 30 g seismic mass are established over the 50–3200 Hz frequency range under controlled sinusoidal excitation with an amplitude of 9.81 m/s^2 (1 g). The resulting detection limits provide a metrologically transparent assessment of the operational sensing capability of the TFPA under the present measurement conditions.

The remainder of this paper is organized as follows. Section II describes the experimental setup and measurement conditions. Section III presents the signal processing methodology used for operational noise estimation and detection limit calculation. Section IV reports the experimental results, which are subsequently discussed in Section V. Finally, the main conclusions of this work are summarized in Section VI.

II. Experimental Setup

A. Device Configuration

The device under investigation is a TFPA previously introduced and characterized in [5]–[7]. The sensing element consists of an open tubular thermo-formed polymer electret structure mechanically coupled to a rigid seismic mass. A schematic representation of the sensing structure is shown in Figure 1.

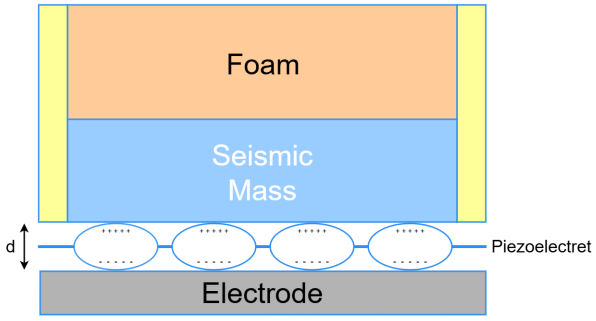

Figure 1. Schematic representation of the TFPA sensing structure.

In the present study, the accelerometer was configured with a seismic mass of 30 g, corresponding to the configuration analyzed in the most recent application-oriented investigation [7]. The electrical output of the TFPA was conditioned using the same signal conditioning chain described in the previous studies to ensure consistency in transduction gain and bandwidth. No modifications were introduced in the sensing structure or conditioning electronics for the present measurements.

B. Excitation Conditions

Dynamic characterization was performed using controlled electrodynamic excitation. The accelerometer was mounted on a vibration exciter together with a reference accelerometer and subjected to sinusoidal acceleration with a nominal amplitude of 1 g. A schematic representation of the experimental setup is shown in Figure 2.

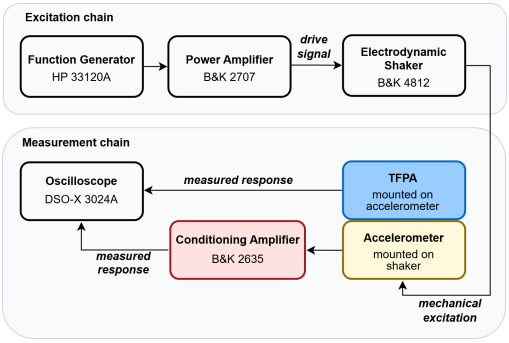

Figure 2. Experimental setup used for dynamic characterization of the TFPA.

Sinusoidal excitation was applied over the frequency range from 50 Hz to 3200 Hz.

The excitation level was monitored using a calibrated Brüel & Kjær 8305 reference accelerometer connected to a B&K 2635 charge amplifier configured with an output sensitivity of 316 mV/g.

C. Data Acquisition

For each excitation condition, three synchronized time-domain signals were recorded:

- time vector t (s),
- output voltage of the reference accelerometer v_{ref} (V),
- output voltage of the TFPA v_{tfpa} (V).

The sampling frequency of each record was determined directly from the time vector as the inverse of the median sampling interval. Since the dataset contains records acquired at different sampling frequencies, this variability is accounted for in the signal processing procedure described in Section III.

III. Signal Processing and Operational Noise Estimation

This section describes the signal processing procedure used to separate deterministic excitation components from stochastic noise in the measured TFPA signals. The methodology includes harmonic regression for removal of the deterministic response, PSD estimation of the residual signal, and the derivation of equivalent acceleration noise density and band-integrated detection limits.

A. Pre-processing and Sensitivity Estimation

For each excitation frequency f_0, the acquired time-domain signals $v_{\mathrm{tfpa}}(t)$ and $v_{\mathrm{ref}}(t)$ were first centered by subtracting their mean value in order to remove DC offsets:

$$v(t) \leftarrow v(t) - \overline{v} \tag{1}$$

where $\overline{v}$ denotes the arithmetic mean over the record duration.

The fundamental amplitude of the TFPA output at the excitation frequency was estimated using harmonic regression. The measured signal was projected onto sine and cosine basis functions at f_0:

$$v_{\mathrm{tfpa}}(t) \approx A_1 \sin(2\pi f_0 t) + B_1 \cos(2\pi f_0 t) \tag{2}$$

The peak amplitude of the fundamental component was then obtained as

$$V_{\mathrm{amp}} = \sqrt{A_1^2 + B_1^2}. \tag{3}$$

Since the excitation amplitude was experimentally adjusted to 1 g peak-to-peak, the corresponding peak acceleration amplitude is $a_p = 0.5$ g. The sensitivity of the accelerometer was therefore calculated as

$$S(f_0) = \frac{V_{\mathrm{amp}}}{0.5\ g} \quad [\mathrm{V/g}]. \tag{4}$$

This procedure was repeated for all excitation frequencies, resulting in a discrete sensitivity curve $S(f_0)$ over the 50–3200 Hz range.

B. Harmonic Regression and Residual Signal Definition

Under sinusoidal excitation, the measured signal may contain higher-order harmonics due to nonlinearities in the sensing structure or conditioning electronics. To isolate the stochastic component, harmonic regression including up to H harmonics was performed:

$$\hat{v}(t) = \sum_{h=1}^{H} \left[A_h \sin(2\pi h f_0 t) + B_h \cos(2\pi h f_0 t) \right]. \tag{5}$$

The number of harmonics was selected as

$$H = \min\left(5, \left\lfloor \frac{F_s/2}{f_0} \right\rfloor\right), \tag{6}$$

ensuring that harmonic components did not exceed the Nyquist frequency while limiting overfitting.

The residual signal, interpreted as operational noise, was defined as

$$r(t) = v_{\mathrm{tfpa}}(t) - \hat{v}(t). \tag{7}$$

C. Power Spectral Density Estimation

The residual signal was analyzed using Welch PSD estimation with a Hann window, segment length of 512 samples, and 50% overlap. The PSD estimate is denoted as

$$P_{rr}(f) \quad [\mathrm{V^2/Hz}]. \tag{8}$$

where $P_{rr}(f)$ denotes the PSD of the residual signal $r(t)$.

The corresponding voltage noise density was computed as

$$S_V(f) = \sqrt{P_{rr}(f)} \quad [\mathrm{V}/\sqrt{\mathrm{Hz}}]. \tag{9}$$

The Welch method provides statistical averaging through segmentation of the residual signal, allowing stable spectral estimation of the noise spectrum.

D. Common Frequency Grid for Heterogeneous Sampling Rates

Measurements acquired at different sampling frequencies lead to PSD estimates with different frequency resolutions and Nyquist limits. To allow consistent aggregation across excitation conditions, the individual PSDs were interpolated onto a common frequency grid.

The common grid was defined using the largest frequency-bin spacing among all records and was limited to the smallest Nyquist frequency observed in the dataset. Each individual spectrum was then mapped onto this grid using piecewise linear interpolation.

The median voltage noise density across all excitation conditions was then computed as

$$S_V^{\mathrm{med}}(f) = \mathrm{median}_i\{S_{V,i}(f)\}, \tag{10}$$

where i indexes the excitation frequencies. The median was adopted as a robust central estimator in order to reduce the influence of occasional residual spectral peaks and inter-record variability.

E. Equivalent Acceleration Noise Density

The frequency-dependent sensitivity curve $S(f)$ was obtained by interpolating the discrete sensitivity estimates $S(f_0)$ onto the common PSD frequency grid using piecewise linear interpolation. The equivalent acceleration noise density was then computed as

$$S_a(f) = \frac{S_V^{\mathrm{med}}(f)}{S(f)} \quad [g/\sqrt{\mathrm{Hz}}]. \tag{11}$$

F. Band-Integrated Detection Limits

The band-integrated RMS acceleration noise over a frequency interval $[f_1, f_2]$ was computed as

$$a_{n,\mathrm{RMS}} = \sqrt{\int_{f_1}^{f_2} S_a^2(f)\, df}. \tag{12}$$

In discrete form,

$$a_{n,\mathrm{RMS}} = \sqrt{\sum_{f_k \in [f_1, f_2]} S_a^2(f_k)\, \Delta f}. \tag{13}$$

The resulting quantity, expressed in g RMS, is defined as the band-integrated operational detection limit for the specified frequency interval.

IV. Results

This section presents the experimental results obtained from the TFPA measurements under controlled sinusoidal excitation. The analysis focuses on three main aspects: the sensitivity of the sensor $S(f)$, the operational noise spectrum $S_V(f)$ obtained from the residual signals after harmonic regression, and the resulting band-integrated detection limits derived from the equivalent acceleration noise density $S_a(f)$.

A. Sensitivity and Signal-to-Noise Ratio

The sensitivity of the TFPA was obtained from the fundamental harmonic amplitude extracted via harmonic regression, according to (4). The resulting sensitivity curve exhibits a pronounced maximum near the resonance region, while the remaining excitation frequencies present substantially lower sensitivity values.

Figure 3 presents the frequency dependence of the TFPA sensitivity obtained from the harmonic regression procedure.

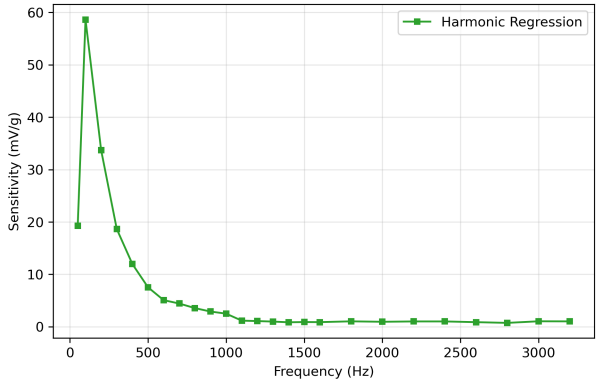

Figure 3. Sensitivity $S(f)$ of the TFPA obtained from harmonic regression.

To evaluate the consistency of the sensitivity estimation procedure, the sensitivity obtained directly from the time-domain [7] was compared with the sensitivity derived from the fundamental component estimated through harmonic regression. The comparison between both estimates is shown in Figure 4.

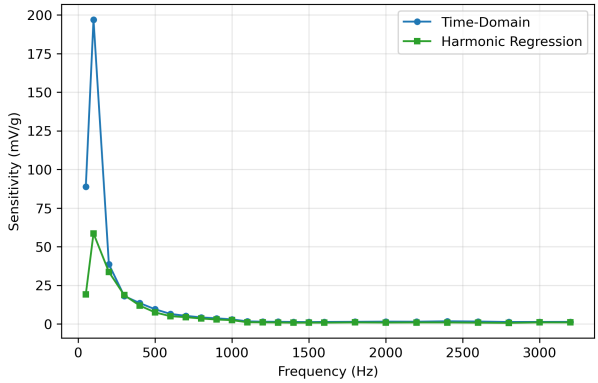

Figure 4. Comparison between TFPA's sensitivity estimated directly from the time-domain signal and from harmonic regression of the fundamental component.

Across the analyzed excitation frequencies between 50 Hz and 3200 Hz, the Signal-to-Noise Ratio (SNR), defined as the ratio between the deterministic fundamental amplitude and the RMS residual noise level, varied between approximately 12.6 dB and 43.1 dB. These values indicate that the deterministic component of the TFPA response remained clearly distinguishable from the residual noise across the analyzed frequency range.

B. Operational Noise Spectral Density

Following harmonic regression, the residual signals were analyzed using Welch PSD estimation. The resulting voltage noise densities $S_V(f)$ from all excitation conditions were interpolated onto a common frequency grid and aggregated using the median estimator (10).

To assess whether the observed spectral levels were dominated by the TFPA or by the measurement chain, the voltage noise density was compared with that of the reference accelerometer channel. Figure 5 presents this comparison.

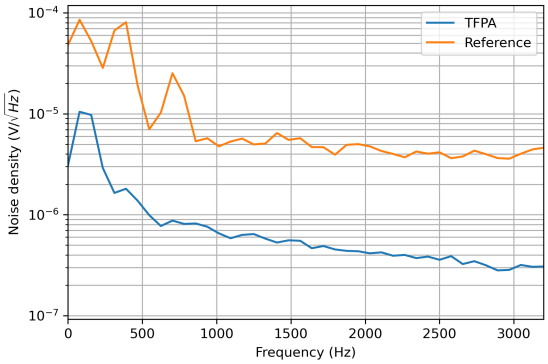

Figure 5. Comparison between the voltage noise density $S_V(f)$ of the TFPA channel and the reference accelerometer channel.

The median voltage noise density exhibited an overall decreasing trend with increasing frequency. At low frequencies near 78 Hz, the median voltage noise density was approximately 1.05×10^{-5} V/$\sqrt{\text{Hz}}$.

Across the analyzed frequency range, the voltage noise density measured at the TFPA output remained consistently below the noise level observed in the reference channel. This result indicates that the TFPA measurement channel exhibited a lower voltage noise density than the reference measurement channel under the present experimental conditions. In this context, the reported noise floor should be interpreted as an operational measurement result of the complete sensing setup, rather than as a fully isolated estimate of the intrinsic TFPA transduction noise.

Using the interpolated sensitivity curve $S(f)$, the voltage noise density $S_V(f)$ was converted into equivalent acceleration noise density $S_a(f)$ according to (11). Figure 6 presents the resulting equivalent acceleration noise spectrum.

Across the analyzed frequency range up to 3200 Hz, the median equivalent acceleration noise density remained on the order of 10^{-4} g/$\sqrt{\text{Hz}}$, with typical values around 1.5×10^{-4} g/$\sqrt{\text{Hz}}$ in the mid-frequency region.

C. Band-Integrated Detection Limits

Band-integrated detection limits were computed by integrating the equivalent acceleration noise density $S_a(f)$ over specified frequency intervals according to (13). The resulting RMS acceleration noise defines the operational detection limit for each band.

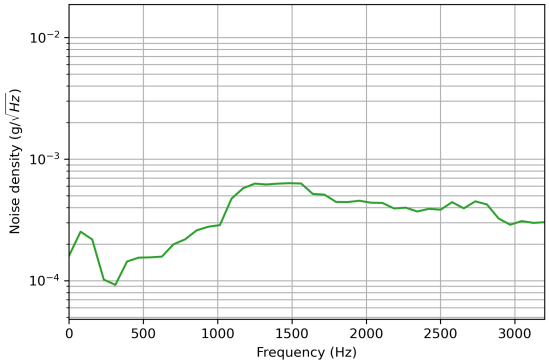

Figure 6. Equivalent acceleration noise density $S_a(f)$ obtained from the TFPA voltage noise density $S_V(f)$ using the interpolated sensitivity curve $S(f)$.

For a detection criterion corresponding to SNR = 1, the resulting detection limits were:

- 3.09 mg RMS for the 50–250 Hz band,
- 3.70 mg RMS for the 50–500 Hz band,
- 22.42 mg RMS for the full 50–3200 Hz band.

When adopting a more conservative detection criterion of SNR = 3, the corresponding detection limits increased to:

- 9.26 mg RMS (50–250 Hz),
- 11.10 mg RMS (50–500 Hz),
- 67.25 mg RMS (50–3200 Hz).

Figure 7 summarizes the resulting detection limits for the analyzed frequency bands.

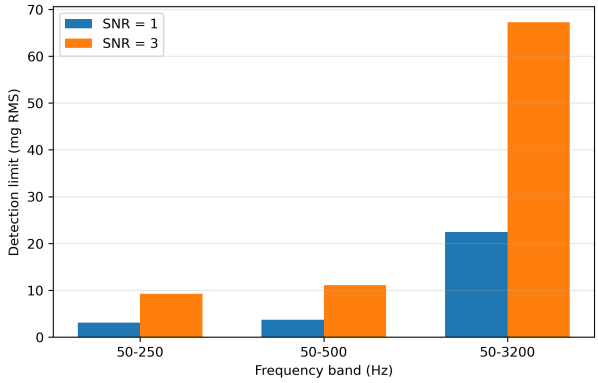

Figure 7. Band-integrated detection limits of the TFPA for different frequency bands and detection criteria.

As expected, the detection limit increases with the integration bandwidth due to the cumulative contribution of spectral noise components. Nevertheless, within the lower frequency band most relevant for many vibration monitoring applications (50–250 Hz), the TFPA demonstrated operational detection limits on the order of only a few milligravity RMS.

These results provide a quantitative assessment of the operational sensing capability of the TFPA and complement the sensitivity and tunability characteristics previously reported for this device architecture.

V. Discussion

This section interprets the experimental results in terms of the sensing characteristics and operational behavior of the TFPA. In particular, the sensitivity, stochastic noise behavior, and band-integrated detection limits are analyzed to assess the practical vibration sensing capability of the device.

A. Sensitivity Characteristics

The experimentally observed sensitivity exhibits a pronounced dependence on excitation frequency. This behavior is consistent with the expected dynamics of a mass–spring sensing structure, in which the mechanical transfer function varies across the analyzed frequency range.

Such sensitivity variation was previously reported for the TFPA architecture and attributed to the dynamic interaction between the thermo-formed electret structure and the seismic mass [6]. The present results confirm that this behavior persists under the operational conditions used for noise characterization.

To evaluate the consistency of the sensitivity estimation procedure, the sensitivity obtained directly from the time-domain signal was compared with the sensitivity derived from the fundamental component estimated through harmonic regression, as shown in Figure 4.

A strong agreement between the two estimates is observed over most of the analyzed frequency range, indicating that the deterministic component of the TFPA response is well captured by the harmonic model. Larger deviations occur near the resonance region, where the estimate derived from the time-domain signal tends to exceed the fundamental-based estimate. This behavior suggests that the waveform departs from a purely sinusoidal shape under dynamic amplification, likely due to increased harmonic content and residual waveform distortion.

The wide dynamic range of sensitivity observed across the analyzed frequency range also reflects the tunable nature of the TFPA concept. As demonstrated in previous work [7], modifications of the seismic mass or structural geometry allow the operational response of the sensor to be shifted toward application-specific frequency bands.

B. Operational Noise Behavior

The spectral analysis of the residual signals revealed a stable operational noise floor across the analyzed frequency range after removal of the deterministic excitation components. The remaining stochastic component of the TFPA signal exhibited a broadband spectral distribution, as illustrated in Figure 5 and Figure 6.

The use of Welch PSD estimation introduces statistical averaging through segmentation of the residual signal, which contributes to the stability of the spectral estimates obtained from each measurement record.

The voltage noise density generally decreased with increasing frequency, reflecting the combined influence of the sensor transduction mechanism and the electronic measurement chain. When converted to equivalent acceleration units using

the sensitivity, the resulting noise spectrum remained within the order of 10^{-4} $\mathrm{g}/\sqrt{\mathrm{Hz}}$ over most of the analyzed range.

A reduction in the equivalent acceleration noise can be observed near the resonance region. This behavior results from the increase in mechanical sensitivity in that frequency range. Since the equivalent acceleration noise density is obtained by dividing the voltage noise density by the sensitivity, the enhanced transduction gain effectively reduces the acceleration-equivalent noise level near resonance.

An important observation arises from the comparison between the TFPA noise spectrum and the reference accelerometer channel shown in Figure 5. Across the evaluated frequency bands, the voltage noise density measured at the TFPA output remained consistently lower than that observed in the reference channel, with clearly distinct residual spectral levels under the present experimental conditions. This comparison indicates that the residual spectral levels depend on the implemented measurement channel, and that the reported noise floor should not be interpreted as a fully isolated estimate of the intrinsic TFPA transduction noise, but rather as an operational result of the TFPA measurement chain.

C. Band-integrated detection limits

The band-integrated detection limits obtained in this study provide a practical measure of the operational sensing capability of the TFPA. While the spectral noise density characterizes the stochastic behavior of the sensor at individual frequencies, the integrated RMS acceleration noise quantifies the minimum detectable vibration level over a specified frequency band.

As expected, the detection limit increases with the integration bandwidth due to the cumulative contribution of spectral noise components. This behavior reflects the broadband nature of the residual noise spectrum observed after removal of the deterministic excitation.

Within the lower frequency band analyzed (50–250 Hz), the TFPA demonstrated a detection limit of approximately 3.09 mg RMS for a unity SNR criterion. Even when adopting a more conservative threshold (SNR = 3), the corresponding detection limit remains below 10 mg RMS in this band. These values indicate that the sensor is capable of resolving vibration levels in the milligravity range when operating within moderate bandwidths.

An important aspect of the obtained detection limits is that they were derived from operational measurements performed under controlled sinusoidal excitation. In this context, the reported values represent operational detection limits that incorporate not only the intrinsic sensor response but also the influence of the measurement chain and the experimental excitation environment. As such, they provide a realistic assessment of the detection capability that can be expected when the device operates in practical measurement conditions.

D. Implications for TFPA-based sensing applications

The results presented in this study extend the characterization of the TFPA beyond sensitivity and structural tunability by providing a quantitative assessment of its operational noise behavior and detection capability. While previous investigations established the design, dynamic response, and application-oriented tunability of the TFPA [5]–[7], the present work adds an evaluation of its operational stochastic detection limits.

In particular, the operational detection limits derived from the residual spectral analysis provide an estimate of the minimum vibration levels that can be resolved under realistic measurement conditions. The results indicate that the TFPA is capable of detecting acceleration levels in the milligravity range within moderate bandwidths, which are typical of many practical vibration monitoring scenarios.

This capability is especially relevant for applications involving low-cost or distributed sensing systems, where lightweight and mechanically tunable sensors can provide useful vibration information without requiring complex instrumentation. In such contexts, the combination of tunable frequency response, milligravity-level detection limits, and simple electromechanical architecture makes the TFPA a relevant candidate for vibration monitoring tasks in environments where traditional sensing solutions may be impractical or cost-prohibitive.

VI. Conclusion and Future Work

This work presented an operational noise characterization and band-integrated detection limit analysis of a TFPA under controlled sinusoidal excitation. A signal processing framework based on harmonic regression was employed to separate deterministic excitation components from stochastic noise, allowing the residual signal to be analyzed using PSD estimation.

The results demonstrated that the TFPA exhibits a sensitivity consistent with the dynamic behavior of a mass–spring sensing structure, while maintaining a stable operational noise floor across the analyzed frequency range. The equivalent acceleration noise density remained on the order of 10^{-4} $\mathrm{g}/\sqrt{\mathrm{Hz}}$, leading to band-integrated detection limits of approximately 3.09 mg RMS in the 50–250 Hz band and 22.42 mg RMS over the full 50–3200 Hz range for a unity SNR criterion.

These results provide a quantitative assessment of the operational vibration detection capability of the TFPA. The present noise characterization helps establish the operational performance limits of the device and contributes to a more complete evaluation of its potential as a mechanically tunable accelerometer architecture for practical vibration sensing applications.

The present study is limited to one TFPA configuration with a 30 g seismic mass and one excitation level of 1 g over the analyzed frequency range. Repeatability across repeated runs, specimen-to-specimen variability, uncertainty quantification, and sensitivity to processing choices were not exhaustively investigated here and should be addressed in future work. Further studies may also investigate approaches to better separate the intrinsic sensor noise from the contribution of the conditioning and acquisition chain.

REFERENCES

[1] M. M. Moreira et al., "Piezoelectrets: A brief introduction," *IEEE Sensors Journal*, vol. 21, pp. 22 317–22 328, 2021.

[2] R. A. Altafim et al., "Piezoelectrets from thermo-formed bubble structures of fluoropolymer- electret films," *IEEE Transactions on Dielectrics and Electrical Insulation*, vol. 13, pp. 979–984, 5 2006.

[3] R. A. P. Altafim et al., "Template-based fluoroethylenepropylene piezoelectrets with tubular channels for transducer applications," *Journal of Applied Physics*, vol. 106, p. 014 106, 2009.

[4] J. F. Alves et al., "An accelerometer based on thermoformed piezoelectrets with open-tubular channels," *Annual Report - Conference on Electrical Insulation and Dielectric Phenomena, CEIDP*, vol. 2020-October, pp. 524–526, 2020.

[5] I. N. Soares et al., "New design for a thermo-formed piezoelectret-based accelerometer," in *ALLSENSORS 2023, The Eighth International Conference on Advances in Sensors, Actuators, Metering and Sensing*, IARIA, 2023, pp. 21–24.

[6] I. N. Soares, R. A. C. Altafim, R. A. P. Altafim, and M. M. Tokoro, "Investigation of thermo-formed piezoelectret accelerometer under different electrodynamic vibration conditions," in *ALLSENSORS 2024, The Ninth International Conference on Advances in Sensors, Actuators, Metering and Sensing*, IARIA, 2024, pp. 32–37.

[7] I. N. Soares, R. A. C. Altafim, and R. A. P. Altafim, "Applicability assessment of a thermo-formed piezoelectret accelerometer in agricultural robotics systems," in *ALLSENSORS 2025, The Tenth International Conference on Advances in Sensors, Actuators, Metering and Sensing*, IARIA, 2025, pp. 19–25.

[8] J. Hillenbrand, S. Haberzettl, T. Motz, and G. M. Sessler, "Electret accelerometers: Physics and dynamic characterization," *The Journal of the Acoustical Society of America*, vol. 129, no. 6, pp. 3682–3689, Jun. 2011.

[9] C. D. Motchenbacher and J. A. Connelly, *Low-noise electronic system design*. Nashville, TN: John Wiley & Sons, 1993.

[10] D. B. Percival and A. T. Walden, *Spectral Analysis for Physical Applications*. Cambridge, England: Cambridge University Press, 1993.

[11] J. Bendat and A. Piersol, *Random Data: Analysis and Measurement Procedures*, Fourth Edition. Wiley, 2010.